PAPER

Nesting and degeneracy of Mie resonances of dielectric cavities within zero-index materials

To cite this article: Xueke Duan *et al* 2022 *J. Opt.* **24** 025401

IOP Publishing Journal of Optics
J. Opt. **24** (2022) 025401 (9pp) https://doi.org/10.1088/2040-8986/ac440c

Nesting and degeneracy of Mie resonances of dielectric cavities within zero-index materials

Xueke Duan[1,6], Haoxiang Chen[1,6], Yun Ma[1,6], Zhiyuan Qian[1], Qi Zhang[1], Yun Lai[5], Ruwen Peng[5], Qihuang Gong[1,2,3,4] and Ying Gu[1,2,3,4,*]

[1] State Key Laboratory for Mesoscopic Physics, Department of Physics, Peking University, Beijing 100871, People's Republic of China
[2] Frontiers Science Center for Nano-optoelectronics & Collaborative Innovation Center of Quantum Matter & Beijing Academy of Quantum Information Sciences, Peking University, Beijing 100871, People's Republic of China
[3] Collaborative Innovation Center of Extreme Optics, Shanxi University, Taiyuan, Shanxi 030006, People's Republic of China
[4] Peking University Yangtze Delta Institute of Optoelectronics, Nantong 226010, People's Republic of China
[5] National Laboratory of Solid State Microstructures, School of Physics, and Collaborative Innovation Center of Advanced Microstructures, Nanjing University, Nanjing 210093, People's Republic of China

E-mail: ygu@pku.edu.cn

Received 8 October 2021, revised 5 December 2021
Accepted for publication 16 December 2021
Published 4 January 2022

Abstract

Resonances in optical cavities are used to manipulate light propagation, enhance light–matter interaction, modulate quantum states, and so on. However, the index contrast between the traditional cavities and the host is generally not high, which to some extent limited their performances. By putting dielectric cavities into a host of zero-index materials, index contrast in principle can approach infinity. Here, we analytically deduced Mie resonance conditions at this extreme circumstance. Interestingly, we discovered a so-called resonance nesting effect, in which a set of cavities with different radii can possess the same type of resonance at the same wavelength. We also revealed previously unknown degeneracy between the 2^l-TM (2^l-TE) and 2^{l+1}-TE (2^{l+1}-TM) modes for $\varepsilon \approx 0$ ($\mu \approx 0$) material, and the 2^l-TM and 2^l-TE for both $\varepsilon \approx 0$ and $\mu \approx 0$. Such extraordinary resonance nesting and degeneracy provide additional principles to manipulate cavity behaviors.

Supplementary material for this article is available online

Keywords: Mie resonances, zero-index media, purcell effect

(Some figures may appear in colour only in the online journal)

1. Introduction

Zero-index materials (ZIMs) [1, 2], including ε-near-zero (ENZ), μ-near-zero (MNZ), and both ε and μ-near-zero (EMNZ) materials, where ε and μ denote permittivity and permeability, respectively, have attracted great interest. They have been experimentally realized in natural materials [3, 4], engineered dispersion waveguides [5–7], photonic crystals [8], and metamaterials [9–12]. Owing to near-zero ε or μ [1, 2], the electric field will decouple with the magnetic field in ZIMs accompanied by constant phase distribution. These specific materials have many attractive properties, like supercoupling [7, 13–15], directional radiation phase pattern [16], large

[6] These authors contributed equally to this work.
[*] Author to whom any correspondence should be addressed.

optical nonlinearity [17, 18], random control of reflection and refraction [19–22], and resonance 'pinning' effect [3, 23], etc. They have also been used in coherent perfect absorption [24], cloaking [25], waveguide connection [13, 14], optical antennas [3, 23], and so on. However, although some studies have investigated the properties of defects in ZIM, they focus more on the transmission and scattering properties rather than the influence on the cavity modes due to the huge index contrast.

Optical cavities are ubiquitous, whose resonances can be used to manipulate light propagation, enhance light–matter interaction, modulate quantum states, and generate quantum sources, and so on. Owing to the existence of the index (ε, μ) contrast between the cavities and the host, optical responses such as surface plasmon resonance [26–28] and dielectric resonance [29–33] occur, characterized as strong local field enhancement. For example, series of resonances of spherical cavities in non-zero dielectric environment are perfectly figured out by the Mie theory [34–36]. However, traditionally the index contrast is generally not so high, which, to some extent, limits the cavity performances. The ZIMs bestow an opportunity to increase the contrast ratio amazingly towards the infinity. Despite this dramatic change of contrast ratio, only the electric dipole resonance of dielectric cavity has been demonstrated to modify the photon-emitter interaction [37–41]. The behaviors of higher order resonances of dielectric cavities embedded in the ZIMs remain unknown.

Here, we analytically deduce Mie resonance conditions of all orders for dielectric spherical cavities embedded in ENZ, MNZ, and EMNZ background, respectively (figure 1). Unusually, for the same angular mode number l, a series of Mie resonances with different radii can be achieved at a fixed wavelength, so-called the resonance nesting effect. More interestingly, the 2^l-TM (TE) mode of the dielectric cavity has the same resonant frequency as that of its 2^{l+1}-TE (TM) mode for the ENZ (MNZ) material; while for EMNZ material, the resonance degeneracy occurs to be the same for its 2^l-TM and 2^l-TE modes. We also find that the degenerate resonances own different linewidths, in other words, as the order l becomes higher, the linewidth becomes narrower. All the above analytical results are confirmed by the numerical finite element method. The nesting and degeneracy of optical modes originate from the ultrahigh contrast ratio of ε or μ between the cavities and the host. Therefore, these phenomena also exist in non-spherical dielectric cavities surrounded by ZIMs. Owing to the resonance degeneracy of optical modes enabled by ZIMs, the interference or superposition between the modes is expected. The resonance degeneracy and nesting enabled by ZIMs could have potential applications in light manipulation, light–matter interaction, and photonic devices.

2. Mie resonance conditions for all orders

We employ Mie theory [34, 35] to solve the conditions that Mie resonances occur in ZIMs. As shown in figure 1, the dielectric spherical cavity (the white part) with the radius of R and dielectric constant ε_1 and magnetic permeability μ_1 is embedded in the infinite ZIM (the blue part) with ε_2 and

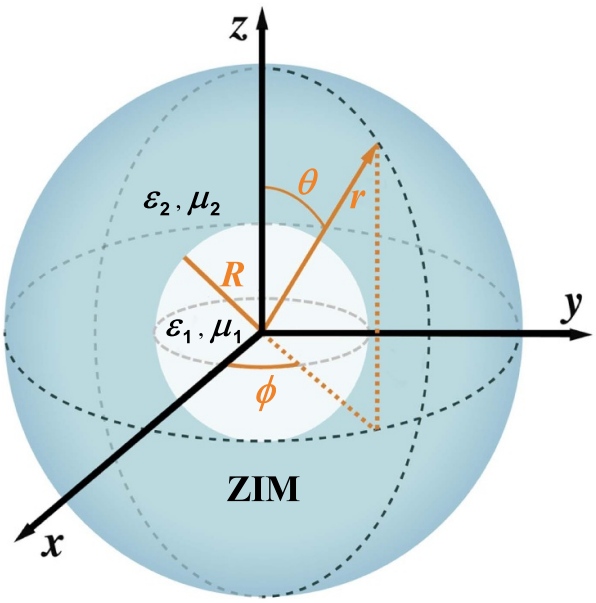

Figure 1. The spherical cavity with zero-index background. The dielectric sphere (the white part) with radius of R embedded in the infinite ZIM (the blue part).

μ_2. Optical modes in the spherical coordinate system are usually labeled as TM_{lm}/TE_{lm} modes [29, 30, 34–36], where TM means transverse magnetic mode and TE transverse electric mode, l the angular mode number, and m the azimuthal mode number satisfying $m \leqslant l$. m has no effect on the resonance conditions, so let $m = 0$. In the following, for simplicity, Mie resonances of the spherical cavity are categorized as 2^l-TM and 2^l-TE Mie resonances, where $l = 1$ denotes the dipole mode and $l = 2$ the quadrupole mode, and so on.

Let us first consider 2^l-TM modes. Because their magnetic field has no radial component, the electromagnetic fields inside and outside the spherical cavity can be written as (see supplementary material available online at stacks.iop.org/JOPT/24/025401/mmedia):

$$\mathbf{H}^l_{\mathrm{TM}} = \begin{cases} \mathbf{M}_l^{(2)} + a\mathbf{M}_l^{(1)}, & r < R, \\ c\mathbf{M}_l^{(3)}, & r \geqslant R, \end{cases}$$
$$\mathbf{E}^l_{\mathrm{TM}} = \begin{cases} -\dfrac{k_1}{i\varepsilon_1\varepsilon_0\omega}\left(\mathbf{N}_l^{(2)} + a\mathbf{N}_l^{(1)}\right), & r < R, \\ -\dfrac{k_2}{i\varepsilon_2\varepsilon_0\omega}\left(c\mathbf{N}_l^{(3)}\right), & r \geqslant R, \end{cases} \tag{1}$$

where a and c are coefficients to be determined, $\mathbf{M}$ and $\mathbf{N}$ are two sets of Mie bases [34–36] on which the electromagnetic field can be expanded. $\mathbf{M}_l^{(j=1,2,3)} = -\frac{\partial \mathrm{P}_l}{\partial\theta} z_l^{(j)}(x)\hat{\mathbf{e}}_\phi$, and $\mathbf{N}_l^{(j=1,2,3)} = \frac{z_l^{(j)}(x)}{x} l(l+1)\mathrm{P}_l\hat{\mathbf{e}}_r + \frac{1}{x}\frac{\partial\left[xz_l^{(j)}(x)\right]}{\partial x}\frac{\partial \mathrm{P}_l}{\partial\theta}\hat{\mathbf{e}}_\theta$, in which $x = kr$ and k is the wavenumber, labeled as k_1 in the sphere and k_2 out the sphere; $z_l^{(j)}$ mean different kinds of spherical harmonic functions respectively: spherical Bessel function j_l, spherical Neumann function n_l, and spherical Hankel function of the first kind $h_l^{(1)}$ which is a linear combination of j_l and n_l, i.e. $h_l^{(1)} = j_l + in_l$. For simplicity, we make

$\eta_l(x) \equiv xj_l(x), \zeta_l(x) \equiv xn_l(x), \xi_l(x) \equiv xh_l^{(1)}(x)$. P_l is the associated Legendre function.

According to the continuity of tangential electric field and magnetic field on the boundary ($r = R$), two linear equations with two coefficients a and c are obtained (see supplementary material):

$$\begin{cases} \tilde{\varepsilon}\left(\zeta_l'(\rho) + a\eta_l'(\rho)\right) = c\xi_l'(s\rho), \\ \zeta_l(\rho) + a\eta_l(\rho) = c\dfrac{\xi_l(s\rho)}{s}, \end{cases} \tag{2}$$

in which $\rho = k_1 R$, $\tilde{\varepsilon} = \varepsilon_2/\varepsilon_1, \tilde{\mu} = \mu_2/\mu_1, s = k_2/k_1 = \sqrt{\tilde{\varepsilon}\tilde{\mu}}$.

When the spherical cavity is resonant, a and c would go to extrema, that is, the denominators of a and c should be zero, which satisfies that:

$$\tilde{\varepsilon}\eta_l'(\rho)\xi_l(s\rho) = s\eta_l(\rho)\xi_l'(s\rho). \tag{3}$$

This is a universal condition that all order TM Mie resonances occur in the spherical cavity embedded in arbitrary medium [36]. When $s \approx 0$, equation (3) turns into the resonance condition of the spherical cavity in ZIMs. And if $s \approx 0$, $\xi_l(s\rho) \approx a_l(s\rho)^{-l}$ and $\xi_l'(s\rho) \approx (-l)a_l(s\rho)^{-(l+1)}$ (see supplementary material), substituting them into equation (3), we obtain:

$$\tilde{\varepsilon}\rho\eta_l'(\rho) + l\eta_l(\rho) = 0, \tag{4}$$

which is the ideal Mie resonance condition for the 2^l-TM modes of spherical cavity embedded in ZIMs. Furthermore, for the ENZ and EMNZ media, $\tilde{\varepsilon} \approx 0$, so equation (4) can be simplified to $\eta_l(\rho) = 0$. Ideal resonance conditions can only be achieved when $s = 0$ or s is very near zero, but in fact, the small imaginary part of ε_2 or μ_2 will make a little influence on the 2^l-TM Mie resonances (see supplementary material).

It is worth mentioning that in addition to ZIMs, $s \approx 0$ can also be satisfied by the situation that $\varepsilon_1 \gg \varepsilon_2$, i.e. the high index cavity embedded in low index material (like air). However, as discussed in supplementary material, the same resonant conditions as above can be achieved only when ε_1 is very high (more than 900).

Then, with the same procedure, the resonance conditions for 2^l-TE modes in the spherical cavity are derived from the continuity of the electromagnetic fields on the boundary ($r = R$). Their electromagnetic fields inside and outside the sphere are written as (see supplementary material):

$$\begin{aligned} \mathbf{E}_{\mathrm{TE}}^l &= \begin{cases} \mathbf{M}_l^{(2)} + b\mathbf{M}_l^{(1)}, & r < R, \\ d\mathbf{M}_l^{(3)}, & r \geqslant R, \end{cases} \\ \mathbf{H}_{\mathrm{TE}}^l &= \begin{cases} \dfrac{k_1}{i\mu_1\mu_0\omega}\left(\mathbf{N}_l^{(2)} + b\mathbf{N}_l^{(1)}\right), & r < R, \\ \dfrac{k_2}{i\mu_2\mu_0\omega}\left(d\mathbf{N}_l^{(3)}\right), & r \geqslant R, \end{cases} \end{aligned} \tag{5}$$

where b and d are coefficients to be determined. According to the continuity of tangential electric field and magnetic field on the boundary ($r = R$), for the 2^l-TE modes we can get a set of linear equations with two unknown coefficients b and d (see supplementary material):

$$\begin{cases} \tilde{\mu}\left(\zeta_l'(\rho) + b\eta_l'(\rho)\right) = d\xi_l'(s\rho), \\ \zeta_l(\rho) + b\eta_l(\rho) = \dfrac{1}{s}d\xi_l(s\rho). \end{cases} \tag{6}$$

When in resonant, the denominators of the coefficients of b and d should be zero, i.e.

$$\tilde{\mu}\eta_l'(\rho)\xi_l(s\rho) = s\eta_l(\rho)\xi_l'(s\rho). \tag{7}$$

Which is a universal condition of all order TE Mie resonances in the spherical cavity embedded in arbitrary medium [36]. While for ZIM medium, $s \approx 0$. In this case, take further simplification of $\xi_l(s\rho)$, and we can get:

$$\tilde{\mu}\rho\eta_l'(\rho) + l\eta_l(\rho) = 0, \tag{8}$$

which is the ideal Mie resonance condition for the 2^l-TE modes of spherical cavity embedded in ZIMs. Specially, for MNZ and EMNZ media, $\tilde{\mu} \approx 0$, so equation (8) can be simplified to $\eta_l(\rho) = 0$. Similarly, the small imaginary part of ε_2 or μ_2 will have effect on the 2^l-TE Mie resonances but different with that on the 2^l-TM Mie resonances (see supplementary material). One can see more details of Mie theory in supplementary material.

The universality of Mie resonance conditions (equation (4) for TM modes and equation (8) for TE modes) is worth to be emphasized. First, these formulas can be applied to all electromagnetic wavelengths like the visible, near-infrared band, microwave, and terahertz though in the following only the examples of visible are illustrated. Second, the spherical cavity inside ZIMs can be any no-zero index materials, rather than the air cavity studied here. Through some appropriate correction, equations (4) and (8) may be applied to some other cavities with spherical symmetry in ZIMs. And it is worth connecting these TE/TM modes with effective index n_{eff} [42], as it will be more intuitive in physics. In the concept of effective index n_{eff}, $\lambda = 2\pi R n_{eff}$. While in our formulas, $\rho = 2\pi R n/\lambda$ where n is the refractive index of the cavity. Through the transformation, it is found that $n_{eff} = n/\rho$, where ρ is the analytical solutions of equations (4) and (8). So effective index n_{eff} can be solved with those resonance conditions. Now for the dielectric cavities in zero index materials, there are several series of solutions for equations (4) and (8), so we can obtain different values of n_{eff}, which corresponds to the resonance nesting and degeneracy.

3. Nesting and degeneracy of Mie resonances

The Mie resonance conditions for 2^l-TM and 2^l-TE modes of dielectric spherical cavity placed in ENZ, MNZ, or EMNZ media are summarized in table 1. When the background varies from ENZ to EMNZ, the resonance conditions of the 2^l-TM modes have no change, but that of the 2^l-TE modes are modulated and become the same as the 2^l-TM modes when μ_2 is also near zero. For the MNZ background, vice versa (see supplementary material). It can be seen that these resonance conditions are related to $\eta_l(\rho)$ and its derivative $\eta_l'(\rho)$. Give the expression of $\eta_l(\rho)$ with $l = 1, 2, 3$:

Table 1. The Mie resonance conditions for 2^l-TM and 2^l-TE modes of dielectric spherical cavity embedded in ZIMs. Here $\rho = k_1 R = 2\pi n R/\lambda$ with the refractive index $n = \sqrt{\varepsilon_1\,\mu_1}$ of dielectric spherical cavity.

	ENZ	MNZ	EMNZ
2^l-TM mode	$\eta_l(\rho) = 0$	$\tilde{\varepsilon}\rho\eta_l'(\rho) + l\eta_l(\rho) = 0$	$\eta_l(\rho) = 0$
2^l-TE mode	$\tilde{\mu}\rho\eta_l'(\rho) + l\eta_l(\rho) = 0$	$\eta_l(\rho) = 0$	$\eta_l(\rho) = 0$

Table 2. The Mie resonance conditions for 2-, 4- and 8-TM/TE modes of dielectric spherical cavity embedded in ZIM.

	2-TM	2-TE	4-TM	4-TE	8-TM	8-TE	…
ENZ ($\mu_2 = \mu_1$)	A	B	C	A	D	C	…
MNZ ($\varepsilon_2 = \varepsilon_1$)	B	A	A	C	C	D	…
EMNZ	A	A	C	C	D	D	…

A: $\sin\rho - \rho\cos\rho = 0$;
B: $\sin\rho = 0$;
C: $(3-\rho^2)\sin\rho - 3\rho\cos\rho = 0$;
D: $(15-6\rho^2)\sin\rho - (15\rho-\rho^3)\cos\rho = 0$.

$$\eta_1(\rho) = \rho^{-1}(\sin\rho - \rho\cos\rho),$$
$$\eta_2(\rho) = \rho^{-2}\left[\left(3-\rho^2\right)\sin\rho - 3\,\rho\cos\rho\right],$$
$$\eta_3(\rho) = \rho^{-3}\left[\left(15-6\rho^2\right)\sin\rho - \left(15\,\rho-\rho^3\right)\cos\rho\right]. \quad (9)$$

Using equation (9) and table 1, the specific resonance conditions for 2-, 4-, and 8-TE/TM modes are listed in table 2. For conciseness, we use A to indicate $\sin\rho - \rho\cos\rho = 0$, B to $\sin\rho = 0$, C to $(3-\rho^2)\sin\rho - 3\rho\cos\rho = 0$ and D to $(15-6\rho^2)\sin\rho - (15\rho-\rho^3)\cos\rho = 0$. For a specific ρ (here $\rho = k_1 R = 2\pi n R/\lambda$ with the refractive index $n = \sqrt{\varepsilon_1\,\mu_1}$ inside the spherical cavity), there is generally a set of solutions from the calculations of A, B, C or D. Namely, if the optical wavelength is fixed, the same Mie resonance can be achieved in spherical cavities with different radii R, which is called as 'resonance nesting'. More specially, if the refractive index $n = \sqrt{\varepsilon_1\,\mu_1}$ of the sphere is 1, the resonant condition A can be replaced by $R/\lambda = 0.7151, 1.2295\ldots$, B by $R/\lambda = 0.5, 1.0\ldots$, C by $R/\lambda = 0.9173, 1.4475\ldots$, and D by $R/\lambda = 1.1122, 1.6579\ldots$, where λ is the wavelength in the vacuum. All the above results are confirmed by the numerical finite element method (see supplementary material). While when the refractive index n is not 1, the nR/λ will be the above values when resonant.

Different to plasmonic particles embedded in non-zero index media that usually have only one resonant R/λ value for one mode [26–28, 43], in the spherical cavity with ZIM background, there are series of R/λ values for each 2^l-TM/TE Mie resonance. As shown in figure 2, when the resonant wavelength is fixed at 630 nm (take an example, also can be at other wavelengths (see supplementary material)), the radiation power ($P = \oiint \frac{1}{2}\mathrm{Re}(\mathbf{E}^* \times \mathbf{H}) \cdot \mathrm{d}\vec{S}$) spectra of 2-TM resonance for ENZ case are analytically obtained at $R = 451.1$ nm, 776.5 nm, 1096.7 nm…, and the spectra of 2-TE resonance at $R = 315.5$ nm, 631.2 nm, 947.0 nm.... It can be seen from the insets of figure 2(a) (or (b)) that the electric field distributions of the three cavities are consistent in form, which just implies

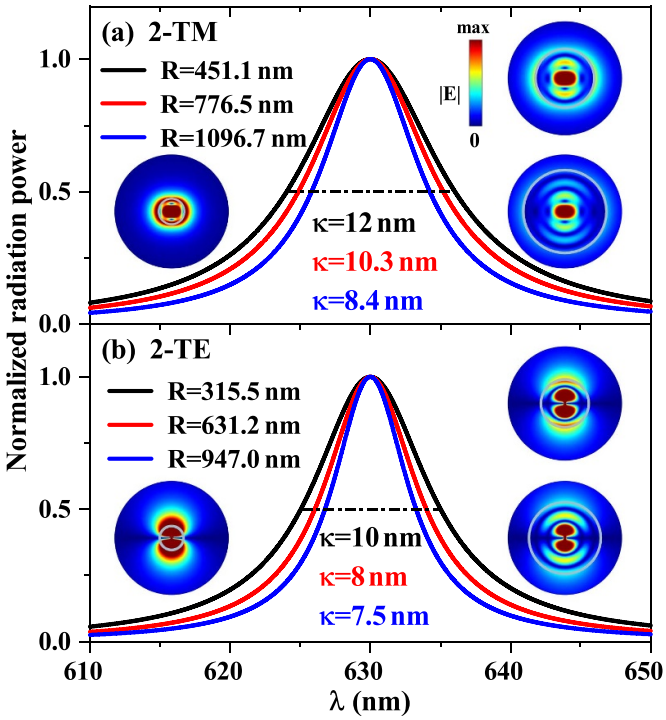

Figure 2. Resonance nesting of (a) 2-TM and (b) 2-TE modes for the air sphere embedded in the ENZ medium when the resonant wavelength is fixed at 630 nm. The insets are corresponding electric field distributions with different R (boundaries are shown as grey circles). Here, ε_2 is set as $0.01\,i$, $\mu_2 = 1$.

these cavities support the same kind of resonance. While the values of cavity loss κ are different, and the larger the cavity, the smaller the loss, because of the increase of lossless energy storage space. It is noted that the resonant R/λ values are a little bigger than ideal values due to the imaginary part of ε_2, and approach ideal values with decreasing the imaginary part (see supplementary material). Besides, the resonance nesting of 2-/4-modes for different ZIMs background is shown in supplementary material.

In addition to the nesting of the same polar mode, there is also the degeneracy between different polar modes. From table 2, it can be seen that for the ENZ case when $\mu_1 = \mu_2$, the 2^l-TM and 2^{l+1}-TE Mie resonances have the same resonance condition, i.e. the same cavity can support both 2^l-TM and 2^{l+1}-TE modes with the same wavelength. Figure 3(a) gives the normalized radiation power spectra of degenerate 2-TM and 4-TE modes in the air cavity with $R = 450.5$ nm embedded in ENZ background with $\varepsilon_2 = 0.01i$ and $\mu_2 = 1$. The little resonance shifts of the two modes originate from the effect of the imaginary part of ε_2 (see supplementary material). Furthermore, the values of κ of the two degenerate modes are different, i.e. $\kappa = 12$ nm for the 2-TM mode but $\kappa = 4$ nm for the 4-TE mode. In a word, the same cavity supports two modes with different loss: the higher the l, the smaller the loss, due to less radiation. The electric field distribution, for 2-TM mode, is discontinuous on the boundary due to the existence of radial component of $\mathbf{E}$ which suddenly changes with the high contrast ratio of ε_2 and ε_1; but for 4-TE mode, the opposite is true (see supplementary material).

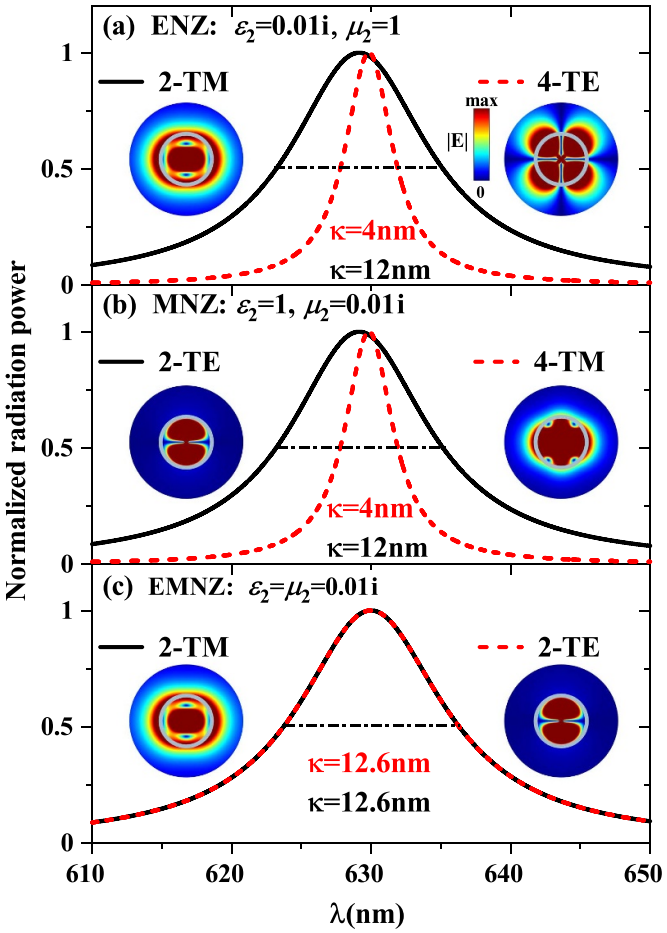

Figure 3. The normalized radiation power spectra of degenerate modes of air spherical cavity with $R = 450.5$ nm in different ZIM: (a) 2-TM and 4-TE modes in ENZ, (b) 2-TE and 4-TM modes in MNZ, and (c) 2-TM and 2-TE modes in EMNZ material. The insets are their electric field distributions.

The resonance degeneracy also happens between the 2^l-TE and 2^{l+1}-TM Mie resonances for the MNZ case when $\varepsilon_1 = \varepsilon_2$ (table 2). As shown in figure 3(b), the normalized radiation power spectra of the 2^l-TE (TM) mode for the MNZ case are the same with that of the 2^l-TM (TE) mode for the ENZ case, because of the symmetry of electromagnetic field expressions. In the same way, the little difference between the resonant wavelength of the 2-TE and 4-TM modes is caused by the influence of the imaginary part of μ_2 (here $\mu_2 = 0.01i$ and $\varepsilon_2 = 1$). The electric field distribution, no matter for 2-TE or 4-TM mode, is continuous on the boundary because $\varepsilon_2 = \varepsilon_1$; and specially for the 2-TE mode, the electric field is almost zero out the sphere. The magnetic field distribution of the 2^l-TM mode of the ENZ case is same as the electric distribution of the 2^l-TE mode of the MNZ case, and vice versa.

While for the EMNZ case, Mie resonance degeneracy occurs between the 2^l-TM and 2^l-TE modes. It can be seen from figure 3(c) that the normalized radiation power spectra for 2-TM and 2-TE modes overlap together with the same cavity loss $\kappa = 12.6$ nm. The electric field distribution of the 2-TM mode has the same form as that in the ENZ case and the 2-TE mode is similar to that in the MNZ case. Although resonance conditions of 2^l-TM mode for ENZ case, 2^l-TE mode for MNZ case and 2^l-TM mode for EMNZ case have the same form, they can not be regarded as degenerate because of the different electromagnetic backgrounds, i.e. different ε_2 and μ_2 in the ZIMs.

4. Discussion

In a cavity made of hyperbolic materials, the electromagnetic field is confined to a small space, where at the same resonant frequency, the same mode can be obtained by hyperbolic metacavities with different sizes due to the anomalous scaling laws [44–46]. But in our study, size-independent has a different meaning. We studied the dielectric sphere cavities embedded in ZIMs. The mode in the dielectric cavity is only related to the radius of the dielectric cavity, no matter how the external boundary of ZIMs changes or the size of ZIMs changes [37], which can be used to manufacture deformable devices.

Since the theory presented here is universal, it can be applied to all the frequency regimes of electromagentic waves, including microwaves, THz and optical frequencies. It is convenient to construct the ZIMs by using the metamaterials or photonic crystals. For instance, the arrays of metallic wires [47] or split rings [48] can tune the effective permittivity or permeability to zero at a certain frequency, respectively. While a dielectric photonic crystal [8] with Dirac-like cones can approximate EMNZ materials. Some semi-conductor materials inherently exhibit near-zero permittivity near their electronic plasma frequency [49].

Now, we discuss the influence of changing the imaginary part $\mathrm{Im}(\varepsilon_2)$ or $\mathrm{Im}(\mu_2)$, i.e. the loss term, on Mie resonances. The ideal resonance conditions listed in table 1 in the main text can be achieved only when $\varepsilon_2 = 0$ or $\mu_2 = 0$. But it is almost impossible to realize the real part and imaginary part both zero. We have the setting that: for ENZ background, μ_2 is 1, the real part of the ε_2 is zero, but the imaginary part has a small value, i.e. $\mu_2 = 1$, $\varepsilon_2 = 0 + \mathrm{Im}(\varepsilon_2)i$; for MNZ background, $\varepsilon_2 = 1$, $\mu_2 = 0 + \mathrm{Im}(\mu_2)i$; while for EMNZ background, $\varepsilon_2 = 0 + \mathrm{Im}(\varepsilon_2)i$, and $\mu_2 = 0 + \mathrm{Im}(\mu_2)i$. From the discussion above, we can see that the small imaginary part would make resonant R/λ have a little deviation from the ideal values.

For the ENZ case, the $\mathrm{Im}(\varepsilon_2)$ affects the resonance wavelengths of both the 2-TM mode and the 4-TE mode. From figures 4(a) and (b), the resonant R/λ values are both coincident with the ideal value $R/\lambda = 0.7151$ for the 2-TM and 4-TE modes only when $\mathrm{Im}(\varepsilon_2)$ is very small. With ε_2 changing from 0.001i to 0.1i, for both 2-TM and 4-TE modes, the resonant R/λ values increase slowly. And the change of the 2-TM mode is a little faster than that of the 4-TE mode. The cavity loss κ also has an obvious increment but still satisfy that the κ of the 2-TM mode is larger than that of the 4-TE mode.

For the MNZ case, changing $\mathrm{Im}(\mu_2)$ of the 2^l-TE (TM) mode has the same effect as changing $\mathrm{Im}(\varepsilon_2)$ of the 2^l-TM (TE) mode for the ENZ case (we do not display the MNZ case in the figure). The resonant R/λ values are both coincident with the ideal value $R/\lambda = 0.7151$ for the 2-TE mode

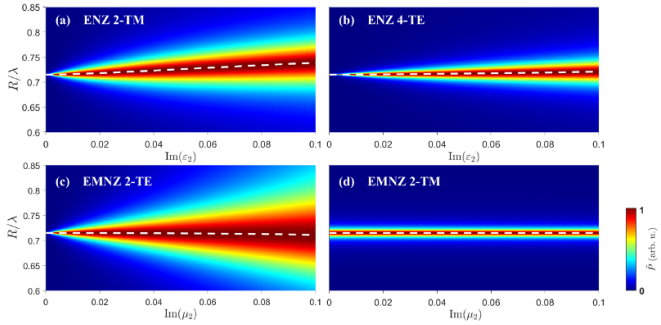

Figure 4. The influence of changing $\mathrm{Im}(\varepsilon_2)$ from 0.001 to 0.1 on the normalized radiation power spectra of Mie resonances of (a) 2-TM mode and (b) 4-TE mode for the ENZ background with $\mu_2 = 1$; changing $\mathrm{Im}(\mu_2)$ from 0.001 to 0.1 on the resonances of (c) 2-TE mode and (d) 2-TM mode for the EMNZ case with $\varepsilon_2 = 0.01i$. The white dot lines are used to represent the resonance wavelengths.

and 4-TM mode when $\mathrm{Im}(\mu_2)$ is very small. With μ_2 changing from 0.001i to 0.1i, for both 2-TE mode and 4-TM mode, the resonant R/λ values increase a little. And the changes of the 2-TE mode are larger than the 4-TM mode. The cavity loss κ also has obvious increment but still satisfies that the κ of the 2-TE mode is larger than that of the 4-TM mode.

For the EMNZ case, figures 4(c) and (d) show the influence of changing the $\mathrm{Im}(\mu_2)$ from 0.001 to 0.1 when $\varepsilon_2 = 0.01i$ on 2-TE mode and 2-TM mode respectively. It can be seen that when $\mathrm{Im}(\mu_2)$ is small, the resonant R/λ values are both coincident with the ideal value $R/\lambda = 0.7151$ for the 2-TE mode and 2-TM mode. As $\mathrm{Im}(\mu_2)$ gets bigger, the resonant R/λ values have a slight decrease for the 2-TE mode, but have almost no change for 2-TM mode; the cavity loss κ becomes bigger for 2-TE mode, and also has almost no change for the 2-TM mode. The weak effect of $\mathrm{Im}(\mu_2)$ on the 2-TM mode comes from the dominant role of small ε_2 in the resonance of 2-TM mode. In the same way, if changing the $\mathrm{Im}(\varepsilon_2)$ from 0.001 to 0.1 when $\mu_2 = 0.01i$, the resonance of the 2-TE mode would has almost no change because of the dominant role of small μ_2 in the resonance of 2-TE mode in this case.

We also discuss the situation of multilayered spherical particles in zero index materials. Previously, multilayer spherical plasmon structures were studied. When the spherical nanoparticle is multilayer, multiple resonances occur through the coupling and hybridization of the electric multipolar modes [50]. For the multilayer plasmon nanoshells, when the shell thickness or dielectric constant is modulated, the resonance peak and linewidth as well as their local field distribution change correspondingly [51, 52]. In the situation that the multilayer dielectric sphere is placed in zero index materials, there will be also attractive phenomena. By designing the thickness of the nanolayer or the dielectric constant of each layer, there also exist the mode coupling and hybridization. Because of resonance nesting and degeneracy existing in our system, accidental degeneracy of optical modes may occur and the near-field localization can be greatly modulated, which may lead to more enhanced the light–matter interaction at the nanoscale.

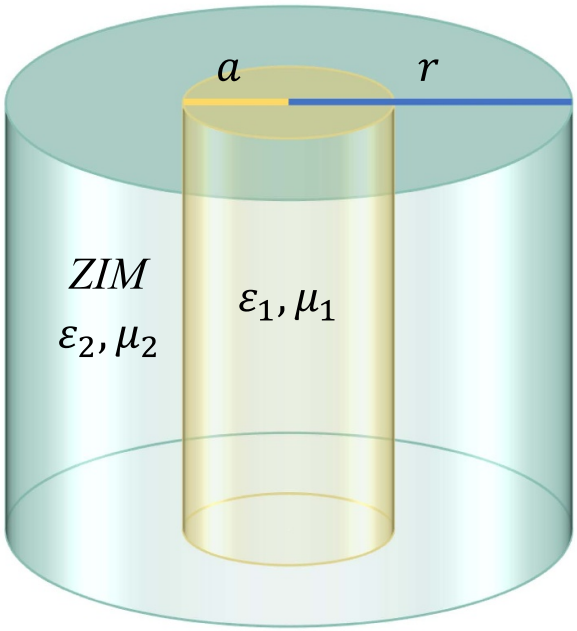

Figure 5. Structures of the 2D cavity. The dielectric cylinder (the yellow part) with the radius of embedded in the infinite ZIM (the green part).

The situation of the 2D structures has also been considered. The 2D structure can be regarded as a ZIMs-wrapped cylindrical cavity, as shown in figure 5. We applied Mie theory in the cylindrical coordinate system and obtained their resonance conditions.

The electric field inside and outside the cavity can be written as:

$$\begin{aligned} E_{in} &= \sum \left(-a_{lm}^{TE} M_{lm} + i a_{lm}^{TM} N_{lm}\right) \\ H_{in} &= \frac{k_1}{\omega \mu_1} \sum \left(a_{lm}^{TM} M_{lm} + i a_{lm}^{TE} N_{lm}\right) \\ E_{out} &= \sum \left(-b_{lm}^{TE} M_{lm} + i b_{lm}^{TM} N_{lm}\right) \\ H_{out} &= \frac{k_2}{\omega \mu_2} \sum \left(b_{lm}^{TM} M_{lm} + i b_{lm}^{TE} N_{lm}\right). \end{aligned} \tag{10}$$

Using boundary continuity conditions, and let $C_1 = \frac{k_1}{\omega \mu_1}$, $C_2 = \frac{k_2}{\omega \mu_2}$, we can obtain the following solutions with cylindrical Bessel functions:

$$\begin{aligned} a_{lm}^{TM} &= \frac{\frac{1}{c_1} H_l'(k_1 r) H_l(k_2 r) - \frac{1}{c_2} H_l(k_1 r) H_l'(k_2 r)}{\frac{1}{c_2} J_l(k_1 r) H_l'(k_2 r) - \frac{1}{c_1} J_l'(k_1 r) H_l(k_2 r)} \\ b_{lm}^{TM} &= \frac{i \frac{k_2}{c_2 \, k_1}}{\frac{1}{c_2} J_l(k_1 r) H_l'(k_2 r) - \frac{1}{c_1} J_l'(k_1 r) H_l(k_2 r)} \\ a_{lm}^{TE} &= \frac{\frac{1}{c_1} H_l(k_1 r) H_l'(k_2 r) - \frac{1}{c_2} H_l'(k_1 r) H_l(k_2 r)}{\frac{1}{c_2} J_l'(k_1 r) H_l(k_2 r) - \frac{1}{c_1} J_l(k_1 r) H_l'(k_2 r)} \\ b_{lm}^{TE} &= -\frac{i \frac{k_2}{c_2 \, k_1}}{\frac{1}{c_2} J_l'(k_1 r) H_l(k_2 r) - \frac{1}{c_1} J_l(k_1 r) H_l'(k_2 r)}. \end{aligned} \tag{11}$$

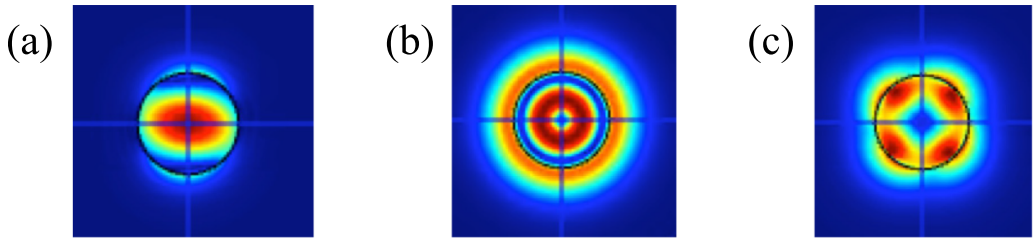

Figure 6. COMSOL simulations of 2D structures: (a) 2-TM mode in ENZ, (b) 2-TE mode in ENZ, (c) 4-TM mode in ENZ.

For TM modes, with a is the radius of the cylinder, the resonance condition is:

$$\frac{1}{c_2}J_l(k_1a)H_l'(k_2a)-\frac{1}{c_1}J_l'(k_1a)H_l(k_2a)=0. \tag{12}$$

When ENZ limit $\varepsilon\sim 0$ is applied:

$$J_l(k_1a)=0. \tag{13}$$

For example, when $l=1$, we obtain:

$$k_1a=3.8317,7.0156,10.1735,\ldots \tag{14}$$

Which means, $\frac{a}{\lambda}=0.6098,1.1166,1.6192,\ldots$, while λ is the resonant wavelength. So resonance nesting happens in 2D cavities. When $l=2$:

$$\frac{a}{\lambda}=0.8174,1.3396,1.8493,\ldots \tag{15}$$

When $l=3$:

$$\frac{a}{\lambda}=1.0154,1.5535,2.0714,\ldots \tag{16}$$

And for TM modes, the resonance condition is:

$$\frac{1}{c_2}J_l'(k_1a)H_l(k_2a)-\frac{1}{c_1}J_l(k_1a)H_l'(k_2a)=0. \tag{17}$$

When ENZ limit is applied:

$$J_l'(k_1a)+\frac{lJ_l(k_1a)}{k_1a}=0. \tag{18}$$

For example, when $l=1$, we obtain:

$$\frac{a}{\lambda}=0.3827,0.8786,1.3773,\ldots \tag{19}$$

When $l=2$:

$$\frac{a}{\lambda}=0.6098,1.1166,1.6192,\ldots \tag{20}$$

When $l=3$:

$$\frac{a}{\lambda}=0.8174,1.3396,1.8493,\ldots \tag{21}$$

From this we know that, for ENZ, 2^l-TM modes is in degenerate with 2^{l+1}-TE modes. And we solved all the cases, then obtained:

	ENZ	MNZ	EMNZ
2^l-TM modes	$J_l(k_1a)=0$	$J_l'(k_1a)+\frac{lJ_l(k_1a)}{k_1a}=0$	$J_l(k_1a)=0$
2^l-TM modes	$J_l'(k_1a)+\frac{lJ_l(k_1a)}{k_1a}=0$	$J_l(k_1a)=0$	$J_l(k_1a)=0$

	2-TM	2-TE	4-TM	4-TE
$ENZ(\mu_1=\mu_2)$	A	B	C	A
$MNZ(\varepsilon_1=\varepsilon_2)$	B	A	A	C
$EMNZ$	A	A	C	C

A: $\frac{a}{\lambda}=0.6098,1.1166,1.6192,\ldots$
B: $\frac{a}{\lambda}=0.3827,0.8786,1.3773,\ldots$
C: $\frac{a}{\lambda}=0.8174,1.3396,1.8493,\ldots$

And different modes of electric field were simulated using COMSOL, as shown in figure 6:

We get resonance nesting and degeneracy results in 2D structures similar to those in sphere cavities.

5. Conclusion

In summary, we have derived analytical expressions of all order Mie resonances occurring for dielectric spherical cavities within the ENZ, MNZ, and EMNZ materials, respectively. Based on these Mie resonance conditions, we have revealed the phenomena of resonance nesting and resonance degeneracy existing in ZIMs. The nesting and degeneracy originate from the high contrast ratio of ε or μ in and out the cavities, thus if the cavities with large ε or μ embedded in the low index materials, the same phenomena will occur (see supplementary material). With resonance nesting, the electric field of the same mode is distributed with different radii, so they can be used to modulate the locality of the field. When a light field or source of the same mode is required, the size of the cavity can be more flexible. Superior to single modes, our degeneracy modes possess coherent coupling of electric fields and so they have potential application in modulating light–matter interaction and light manipulation.In contrast to previous mode degeneracy generally occurring between $+l$ and $-l$, the mode degeneracy here with different angular mode number

l will provide an additional way to realize quantum entanglement and quantum operation. Besides, the modes in the cavity do not vary with the shape or size of the external boundary of the ZIMs [37], so our study can also be applied to deformable devices.

Data availability statement

All data that support the findings of this study are included within the article (and any supplementary files).

Acknowledgments

This work is supported by the National Natural Science Foundation of China under Grant Nos. 11974032, 11525414, 11734001, and 11974176, and by the Key R&D Program of Guangdong Province under Grant No. 2018B030329001.

ORCID iDs

Zhiyuan Qian https://orcid.org/0000-0003-1789-6643
Yun Lai https://orcid.org/0000-0002-0040-9274
Ruwen Peng https://orcid.org/0000-0003-0424-2771
Ying Gu https://orcid.org/0000-0002-0661-5159

References

[1] Liberal I and Engheta N 2017 Near-zero refractive index photonics *Nat. Photon.* **11** 149
[2] Engheta N 2013 Pursuing near-zero response *Science* **340** 286
[3] Kim J *et al* 2016 Role of epsilon-near-zero substrates in the optical response of plasmonic antennas *Optica* **3** 339
[4] Naik G V, Kim J and Boltasseva A 2011 Oxides and nitrides as alternative plasmonic materials in the optical range *Opt. Mater. Express* **1** 1090
[5] Edwards B, Alu A, Young M E, Silveirinha M and Engheta N 2008 Experimental verification of epsilon-near-zero metamaterial coupling and energy squeezing using a microwave waveguide *Phys. Rev. Lett.* **100** 033903
[6] Vesseur E J R, Coenen T, Caglayan H, Engheta N and Polman A 2013 Experimental verification of n=0 structures for visible light *Phys. Rev. Lett.* **110** 013902
[7] Liberal I, Mahmoud A M, Li Y, Edwards B and Engheta N 2017 Photonic doping of epsilon-near-zero media *Science* **355** 1058
[8] Huang X, Lai Y, Hang Z H, Zheng H and Chan C T 2011 Dirac cones induced by accidental degeneracy in photonic crystals and zero-refractive-index materials *Nat. Mater.* **10** 582
[9] Maas R, Parsons J, Engheta N and Polman A 2013 Experimental realization of an epsilon-near-zero metamaterial at visible wavelengths *Nat. Photon.* **7** 907
[10] Moitra P *et al* 2013 Realization of an all-dielectric zero-index optical metamaterial *Nat. Photon.* **7** 791
[11] Li Y *et al* 2015 On-chip zero-index metamaterials *Nat. Photon.* **9** 738
[12] Pollard R J *et al* 2009 Optical nonlocalities and additional waves in epsilon-near-zero metamaterials *Phys. Rev. Lett.* **102** 127405
[13] Silveirinha M G and Engheta N 2007 Theory of supercoupling, squeezing wave energy and field confinement in narrow channels and tight bends using epsilon near-zero metamaterials *Phys. Rev.* B **76** 245109
[14] Silveirinha M and Engheta N 2006 Tunneling of electromagnetic energy through subwavelength channels and bends using epsilon-near-zero materials *Phys. Rev. Lett.* **97** 157403
[15] Marcos J S, Silveirinha M G and Engheta N 2015 μ-near-zero supercoupling *Phys. Rev.* B **91** 195112
[16] Alu A, Silveirinha M G, Salandrino A and Engheta N 2007 Epsilon-near-zero metamaterials and electromagnetic sources: tailoring the radiation phase pattern *Phys. Rev.* B **75** 155410
[17] Alam M Z, Schulz S A, Upham J, De Leon I and Boyd R W 2018 Large optical nonlinearity of nanoantennas coupled to an epsilon-near-zero material *Nat. Photon.* **12** 79
[18] lam M Z, De Leon I and Boyd R W 2016 Large optical nonlinearity of indium tin oxide in its epsilon-near-zero region *Science* **352** 795
[19] Luo J, Li J and Lai Y 2018 Electromagnetic impurity-immunity induced by parity-time symmetry *Phys. Rev.* X **8** 031035
[20] Luo J, Hang Z, Chan C T and Lai Y 2015 Unusual percolation threshold of electromagnetic waves in double-zero medium embedded with random inclusions *Laser Photon. Rev.* **9** 523
[21] Nguyen V C, Chen L and Klaus H 2010 Total transmission and total reflection by zero index metamaterials with defects *Phys. Rev. Lett.* **105** 233908
[22] Liberal I, Li Y and Engheta N 2018 Reconfigurable epsilon-near-zero metasurfaces via photonic doping *Nanophotonics* **7** 1117
[23] Schulz S A *et al* 2016 Optical response of dipole antennas on an epsilon-near-zero substrate *Phys. Rev.* A **93** 063846
[24] Simin F and Klaus H 2012 Coherent perfect absorption in epsilon-near-zero metamaterials *Phys. Rev.* B **86** 165103
[25] Chu H *et al* 2018 A hybrid invisibility cloak based on integration of transparent metasurfaces and zero-index materials *Light Sci. Appl.* **7** 50
[26] Kelly K, Coronado E, Zhao L and Schatz G 2003 The optical properties of metal nanoparticles: the influence of size, shape and dielectric environment *Phys. Chem.* B **107** 668
[27] Kreibig U and Vollmer M 1995 *Optical Properties of Metal Clusters* (Berlin: Springer)
[28] Lian H *et al* 2015 Efficient single photon emission and collection based on excitation of gap surface plasmons *Phys. Rev. Lett.* **114** 193002
[29] Gastine M, Courtols L and DorMann J 1967 Electriomagnetic resonances of free dielectric spheres *IEEE Trans. Microw. Theory Tech.* **MT15** 694
[30] Affolter P and Eliasson B 1973 Electriomagnetic resonances and q-factor of lossy dielectric spheres *IEEE Trans. Microw. Theory Tech.* **MT21** 573
[31] Richtmyer R 1939 Dielectric resonators *J. Appl. Phys.* **10** 391
[32] Jahani S and Jacob Z 2016 All-dielectric metamaterials *Nat. Nanotechnol.* **11** 23
[33] Kuznetsov A I, Miroshnichenko A E, Brongersma M L, Kivshar Y S and Luk'yanchuk B 2016 Optically resonant dielectric nanostructures *Science* **354** 846
[34] Mie G 1908 Articles on the optical characteristics of turbid tubes, especially colloidal metal solutions *Ann. Phys., Lpz.* **25** 377
[35] Debye P 1909 The heliograph of spheres of any material *Ann. Phys., Lpz.* **30** 57
[36] Bohren C F and Huffman D R 1976 *Absorption and Scattering of Light by Small Particles* (New York: Wiley-VCH Verlag GmbH Co. KGaA)
[37] Liberal I, Mahmoud A M and Engheta N 2016 Geometry-invariant resonant cavities *Nat. Commun.* **7** 10989
[38] Liberal I and Engheta N 2017 Zero-index structures as an alternative platform for quantum optics *Proc. Natl Acad. Sci. USA* **114** 822

[39] Silveirinha M G 2014 Trapping light in open plasmonic nanostructures *Phys. Rev.* A **89** 023813
[40] Liberal I and Engheta N 2016 Nonradiating and radiating modes excited by quantum emitters in open epsilon-near-zero cavities *Sci. Adv.* **2** e1600987
[41] Yue L, Liberal I and Engheta N 2019 Structural dispersion–based reduction of loss in epsilon-near-zero and surface plasmon polariton waves *Sci. Adv.* **5** eaav3764
[42] Yang S, Wang Y and Sun H 2015 Advances and prospects for whispering gallery mode microcavities *Adv. Opt. Mater.* **3** 1136
[43] Duan X *et al* 2019 Accumulation and directionality of large spontaneous emission enabled by epsilon-near-zero film *Opt. Express* **27** 7426
[44] Guo Z, Jiang H and Chen H 2022 Zero-index and hyperbolic metacavities: fundamentals and applications *J. Phys. D: Appl. Phys.* **55** 083001
[45] Wang Y, Guo Z, Chen Y, Chen X, Jiang H and Chen H 2020 Circuit-based magnetic hyperbolic cavities *Phys. Rev. Appl.* **13** 044024
[46] Yang X *et al* 2012 Experimental realization of three-dimensional indefinite cavities at the nanoscale with anomalous scaling laws *Nat. Photon.* **6** 450
[47] Pendry J B, Holden A J, Stewart W J and Youngs I 1996 Extremely low frequency plasmons in metallic mesostructures *Phys. Rev. Lett.* **76** 4773
[48] Liu R *et al* 2008 Experimental demonstration of electromagnetic tunneling through an epsilon-near-zero metamaterial at microwave frequencies *Phys. Rev. Lett.* **100** 023903
[49] Vassant S *et al* 2012 Epsilon-near-zero mode for active optoelectronic devices *Phys. Rev. Lett.* **109** 237401
[50] Radloff C and Halas N J 2004 Plasmonic properties of concentric nanoshells *Nano Lett.* **4** 1323
[51] Lal S, Link S and Halas N J 2007 Nano-optics from sensing to waveguiding *Nat. Photon.* **1** 641
[52] Tam F *et al* 2007 Mesoscopic nanoshells: geometry-dependent plasmon resonances beyond the quasistatic limit *J. Chem. Phys.* **127** 204703